Atmospheric Environment 69 (2013) 281–288

Contents lists available at SciVerse ScienceDirect

Atmospheric Environment

journal homepage: www.elsevier.com/locate/atmosenv

Hygroscopic properties of oxalic acid and atmospherically relevant oxalates

Qingxin Ma, Hong He*, Chang Liu

Research Center for Eco-Environmental Sciences, Chinese Academy of Sciences, 18 Shuangqing Road, Haidian District, Beijing 100085, China

HIGHLIGHTS

- ► Hygroscopic behavior of oxalic acid and oxalates were studied under ambient conditions.
- ► No deliquescence and dehydration for oxalates was observed.
- ► All samples studied exhibited hydration during humidifying process.
- ► It suggests that the most stable state for oxalic acid and oxalates is hydrated particles in the atmosphere.

ARTICLE INFO

Article history:
Received 24 April 2012
Received in revised form
11 December 2012
Accepted 12 December 2012

Keywords:
Oxalates
Hygroscopic behavior
Vapor sorption analyzer
Raman spectroscopy

ABSTRACT

Oxalic acid and oxalates represent an important fraction of atmospheric organic aerosols, however, little knowledge about the hygroscopic behavior of these particles is known. In this study, the hygroscopic behavior of oxalic acid and atmospherically relevant oxalates ($H_2C_2O_4$, $(NH_4)_2C_2O_4$, CaC_2O_4, and FeC_2O_4) were studied by Raman spectrometry and vapor sorption analyzer. Under ambient relative humidity (RH) of 10–90%, oxalic acid and these oxalates hardly deliquesce and exhibit low hygroscopicity, however, transformation between anhydrous and hydrated particles was observed during the humidifying and dehumidifying processes. During the water adsorption process, conversion of anhydrous $H_2C_2O_4$, $(NH_4)_2C_2O_4$, CaC_2O_4, and FeC_2O_4 to their hydrated particles (i.e., $H_2C_2O_4\cdot 2H_2O$, $(NH_4)_2C_2O_4\cdot H_2O$, $CaC_2O_4\cdot H_2O$, and $FeC_2O_4\cdot 2H_2O$) occurred at about 20% RH, 55% RH, 10% RH, and 75% RH, respectively. Uptake of water on hydrated Ca-oxalate and Fe-oxalate particles can be described by a multilayer adsorption isotherm. During the dehumidifying process, dehydration of $H_2C_2O_4\cdot 2H_2O$ and $(NH_4)_2C_2O_4\cdot H_2O$ occurred at 5% RH while $CaC_2O_4\cdot H_2O$ and $FeC_2O_4\cdot 2H_2O$ did not undergo dehydration. These results implied that hydrated particles represent the most stable state of oxalic acid and oxalates in the atmosphere. In addition, the assignments of Raman shift bands in the range of 1610–1650 cm^{-1} were discussed according to the hygroscopic behavior measurement results.

1. Introduction

Atmospheric aerosols affect climate directly through scattering and absorption of solar radiation, and indirectly through changing the optical properties and lifetime of clouds by acting as cloud condensation nuclei (CCN) (Charlson et al., 1992; Ramanathan et al., 2001). The global average contribution of the cooling effect of aerosols is almost equivalent to the warming effect of carbon dioxide (IPCC, 2007; Ramanathan et al., 2001). Because of its complexity in composition and chemical transformation, however, aerosol still represents one of the largest current sources of uncertainty in predictions of the future global climate (IPCC, 2007). Thus, a number of studies have been performed on the physicochemical properties of atmospheric particles. Hygroscopicity is one of the most fundamental properties of atmospheric particles, which plays an important role in the deposition characteristics, cloud formation, visibility degradation, and atmospheric chemistry of atmospheric particulate matter (Charlson et al., 1992). There have been a variety of studies focusing on the hygroscopic behavior of atmospherically relevant particles, in which water contents, growth factors, deliquescence and efflorescence points, and morphology as a function of relative humidity were measured. While the hygroscopic properties of inorganic salts commonly found in

* Corresponding author. Tel.: +86 10 62849123; fax: +86 10 62923563.
E-mail address: honghe@rcees.ac.cn (H. He).

1352-2310/$ – see front matter © 2013 Elsevier Ltd. All rights reserved.
http://dx.doi.org/10.1016/j.atmosenv.2012.12.011

atmospheric aerosols are well characterized nowadays, knowledge on the influence of water uptake of the organic aerosol fraction still remains limited (Wu et al., 2011).

Dicarboxylic acids (DCAs, or diacids) are ubiquitous in the atmosphere and represent a significant portion of the organic fraction of aerosols (Chebbi and Carlier, 1996). Due to their strong hydrophilic and hygroscopic properties, dicarboxylic acids are able to reduce the surface tension of cloud condensation nuclei, which consequently affects the cloud formation and the global radiation balance (Kerminen et al., 2000; Kumar et al., 2003; Prenni et al., 2001; Yu, 2000). Oxalic acid ($H_2C_2O_4$) is the most abundant contributor to the total dicarboxylic acid mass in ambient organic aerosol particles, and has been detected in aqueous phases (fog, cloud, and precipitation) and particulate phases (Chebbi and Carlier, 1996; Hsieh et al., 2007; Kerminen et al., 2000; Kawamura et al., 2010; Mochida et al., 2003a; Yang and Yu, 2008; Yao et al., 2002; Yu, 2000). The primary sources of $H_2C_2O_4$ include fossil fuel combustion, biomass burning, and vehicle exhaust while the secondary formation pathways include photo-oxidation of volatile organic compounds (VOC) in gas-phase, aqueous phase, and heterogeneous processes (Carlton et al., 2007; Chebbi and Carlier, 1996; Ervens et al., 2004; Kawamura et al., 2005; Kundu et al., 2010; Mochida et al., 2003a, 2003b; Röhrl and Lammel, 2001; Sorooshian et al., 2006; Wang et al., 2010; Warneck, 2003; Yu, 2000). A high correlation has also been observed between sulfate and oxalate in aerosol collected at various locations, which was likely a result of the potential importance of the in-cloud formation pathway for both sulfate and oxalate (Sorooshian et al., 2007; Yao et al., 2004; Yu et al., 2005).

The hygroscopic behavior of pure $H_2C_2O_4$ has been widely studied. By using an electrodynamic balance (EDB), Peng et al. (2001) determined that oxalic acid does not deliquesce in the range of 10%–90% RH, with little growth of particle size. In another study by aerosol flow tube-FTIR, Braban et al. (2003) reported the conversion of anhydrous oxalic acid to dihydrate at 12% RH and a deliquescence point at ~98% RH for oxalic acid particles at 293 K. Wu et al. (2011) also reported that at 90% RH, oxalic acid does not take up any water. On the other hand, it was determined that oxalic acid can be transformed to oxalate salts during atmospheric transport in oxalic acid-containing mixtures. Recently, field measurement results analyzing Asian dust by single particle mass spectrometry (ATOFMS) showed that $H_2C_2O_4$ was predominantly mixed with mineral dust during transport in the atmosphere (Sullivan and Prather, 2007; Yang et al., 2009). By using X-ray absorption fine structure spectroscopy (XAFS), Furukawa and Takahashi (2011) also found that most of the oxalic acid is present as a metal oxalate complexes in the aerosols, especially as Ca and Zn oxalate complexes. Our previous study confirmed that coexisting hygroscopic components (e.g., $Ca(NO_3)_2$) can enhance the reaction between $H_2C_2O_4$ and calcite during the humidifying process of $Ca(NO_3)_2/CaCO_3/H_2C_2O_4$ mixtures, although direct reaction between $H_2C_2O_4$ and calcite is limited even under humid conditions (Ma and He, 2012). In addition, it is well known that oxalate occurs in many plants and is also the primary constituent of the most common kind of kidney stones (Garty and Garty-Spitz, 2011). Products of the reaction of oxalic acid formed by lichen hyphae and metal ions in the rock substratum have also generated much analytical interest (Edwards et al., 2003). In contrast to oxalic acid, little attention has been paid to the hygroscopic behavior of oxalates. Hence, it is necessary to study the hygroscopic behavior of oxalate salts.

In this study, the hygroscopic behavior of oxalic acid and oxalate including ammonium oxalate, calcium oxalate, and iron oxalate were studied by vapor sorption analyzer and Raman spectroscopy. The present study is helpful for our understanding of the indirect climate effect of oxalic acid and oxalates, as well as the transformation processes of oxalic acid in the atmosphere.

2. Experimental section

2.1. TGA analysis

The thermogravimetric analysis (TGA) thermograms were obtained from a METTLER-TOLEDO (TGA/DSC 1/1600) thermal gravimetry instrument with an accuracy of ±1 μg. The balance and sample compartments were purged with nitrogen. The temperature program was from 30 to 800 °C, with a heating rate of 10 °C min^{-1} in a flow of 50 mL min^{-1} N_2.

2.2. Raman study

Raman spectroscopy has been widely used to investigate the heterogeneous reactions and hygroscopic behavior of atmospheric particles (Dong et al., 2009; Liu et al., 2010; Ma and He, 2012). *In situ* Raman spectra were recorded with a UV resonance Raman spectrometer (UVR DLPC-DL-03), which has been described in a previous article (Liu et al., 2010). Briefly, a continuous diode-pumped solid state (DPSS) laser beam (532 nm) was used as the exciting radiation with source power of 40 mW. The diameter of the laser spot on the sample surface was focused at 25 μm. The spectral resolution was 2.0 cm^{-1}. The instrument was calibrated against the Stokes Raman signal of Teflon at 1378 cm^{-1}. All experiments were conducted at 20 °C. Particles were placed in an *in situ* cell used as a flow reactor. The relative humidity was controlled by adjusting the ratio of dry and humid nitrogen in the gas flow and it was recorded by a moisture meter (CENTER 314, China) with an accuracy ±2% RH and ±0.1 °C. The equilibrium time for each RH point was more than 30 min.

2.3. Vapor sorption analyzer experiments

Water adsorption isotherms were measured with a modified vapor sorption analyzer at 5 °C. The method has been described in a previous article (Ma et al., 2010). Briefly, the vapor sorption analyzer was modified from a N_2 adsorption–desorption analyzer which is used in characterizing the surface area of solid material. Water vapor instead of nitrogen was used as adsorbate in studying the hygroscopicity of particles. The relative humidity (RH) was referred to relative pressure (P/P_0), in which P_0 was set as the saturation vapor pressure at the temperature of the sample. When values of P_0 and RH points were established, then the absolute pressure around the sample was controlled automatically by computer program. By adjusting the speed rate of the turbo pump, the pressure can be controlled at the level of 10^{-4} Torr, which makes the uncertainty less than 1%. For the hygroscopic behavior study, we set the sensitivity of the instrument to yield an uncertainty of 2%, in order to shorten the experiment time. The mixed particles were first ground together and then evacuated at room temperature for 3 h at a pressure of 10^{-3} Torr. The evacuated particles were exposed to vapor with different RH to determine the adsorption isotherm by calculating the pressure change during the equilibrium process.

2.4. Chemicals

$H_2C_2O_4 \cdot 2H_2O$ (AR, >99.5%), $(NH_4)_2C_2O_4 \cdot H_2O$ (AR, >99.8%), and $CaC_2O_4 \cdot H_2O$ (AR, >99.0%) were from Sinopharm Chemical Reagent Co. Ltd. while $FeC_2O_4 \cdot 2H_2O$ (AR, >99%) was from Alfa Aesar. All samples were used as received. Distilled H_2O was degassed by heating prior to use.

3. Results and discussion

3.1. TGA analysis results

We first conducted thermo-decomposition experiments to prepare anhydrous particles because $CaC_2O_4 \cdot H_2O$ and $Fe_2C_2O_4 \cdot 2H_2O$ cannot be dehydrated by dry N_2 purge. Fig. 1 shows the TGA thermograms of $H_2C_2O_4 \cdot 2H_2O$, $(NH_4)_2C_2O_4 \cdot H_2O$, $FeC_2O_4 \cdot 2H_2O$, and $CaC_2O_4 \cdot H_2O$ measured in a flow of N_2 with a heating rate 10 °C min^{-1} from 30 to 800 °C in an alumina sample holder. Calcium oxalate monohydrate ($CaC_2O_4 \cdot H_2O$) is commonly used as a calibration standard for TGA (Chang and Huang, 1997). As seen in Fig. 1 (line a), the weight loss percentages for $CaC_2O_4 \cdot H_2O$ were 12.5%, 31.6%, and 61.4% at about 210 °C, 500 °C, and 780 °C, respectively, which indicated the complete transformations of $CaC_2O_4 \cdot H_2O$ to CaC_2O_4, $CaCO_3$, and CaO. These results were consistent with previously reported results (Chang and Huang, 1997). For $FeC_2O_4 \cdot 2H_2O$ (Fig. 1 line b), the weight loss percentages were 19.8% and 59.5% at 210 °C and 420 °C, respectively, which indicated that the conversion of $FeC_2O_4 \cdot 2H_2O$ to FeC_2O_4 and FeO took place. For $(NH_4)_2C_2O_4 \cdot H_2O$ (Fig. 1 line c) and $H_2C_2O_4 \cdot 2H_2O$ (Fig. 1 line d), the weight loss percentages were 12.5% and 28.5% at about 120 °C, respectively, indicating that the complete dehydration temperature for both $H_2C_2O_4 \cdot 2H_2O$ and $(NH_4)_2C_2O_4 \cdot H_2O$ was about 120 °C. The complete decomposition temperatures of these two components were 200 °C and 290 °C, respectively. In later hygroscopic behavior measurements, anhydrous CaC_2O_4 and FeC_2O_4 particles were prepared by heating hydrated particles according to the TGA results.

3.2. Hygroscopic behavior

3.2.1. Oxalic acid and ammonium oxalate

Under dry or vacuum conditions, $H_2C_2O_4 \cdot 2H_2O$ and $(NH_4)_2C_2O_4 \cdot H_2O$ are dehydrated. Thus, water adsorption isotherms of $H_2C_2O_4 \cdot 2H_2O$ and $(NH_4)_2C_2O_4 \cdot H_2O$ particles could not be measured in this study. Fig. 2 shows the water adsorption isotherms of anhydrous $H_2C_2O_4$ and $(NH_4)_2C_2O_4$ particles measured with the vapor sorption analyzer at 5 °C. For anhydrous $H_2C_2O_4$ particles, the water adsorption isotherm exhibits a transition at ~20% RH. The water content above 20% RH is close to 0.4 g per gram $H_2C_2O_4$ (equal to molar ratio of 2), indicating the formation of the dihydrate of oxalic acid. The discrepancy between the measured value and theoretical value may be due to the diffusion effect of accumulated particles. No deliquescence was observed for anhydrous $H_2C_2O_4$ or dihydrate particles even when RH reached

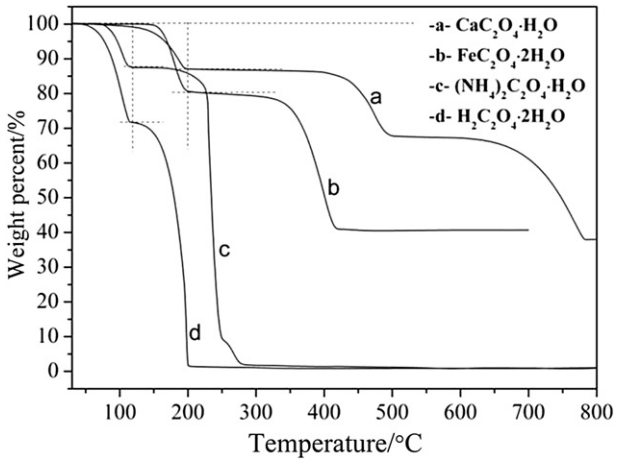

Fig. 1. TGA of oxalic acid and oxalates with a heating rate 10 °C min^{-1} in a flow of N_2.

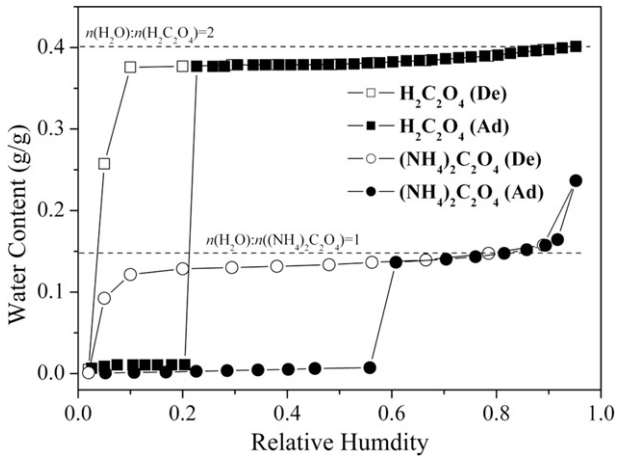

Fig. 2. Water adsorption–desorption isotherms of $H_2C_2O_4$ and $(NH_4)_2C_2O_4$ at 5 °C.

95% RH. The deliquescence relative humidity (DRH) for oxalic acid at ~98% RH was reported in a previous study using FT-IR (Braban et al., 2003). Since the typical RH range in the atmosphere is about 10–90%, this suggests the most common state of atmospheric oxalic acid particle is the solid dihydrate.

For $(NH_4)_2C_2O_4$ particles, little water was taken up at lower RH. As RH increased above 60% RH, the water content exhibited an abrupt increase and reached ~0.14 g per gram $(NH_4)_2C_2O_4$ (equal to a molar ratio of 1), implying the conversion of anhydrous to monohydrate particles. Another abrupt increase was also observed at 95% RH, which may be due to the pre-deliquescence of $(NH_4)_2C_2O_4$. However, the DRH point was not measured due to the RH range limitation of the apparatus (0–95% RH). Peng and Chan (2001) studied the hygroscopic behavior of $(NH_4)_2C_2O_4$ and showed that $(NH_4)_2C_2O_4$ crystallized to form anhydrous particles under dry conditions but did not deliquesce at RH <94%. In a recent study using a hygroscopicity tandem differential mobility analyzer (H-TDMA), Wu et al. (2011) found that the growth factor for $(NH_4)_2C_2O_4$ was 1.05 when RH was above 30%RH and remained constant below 90% RH. We can conclude that under ambient conditions, $(NH_4)_2C_2O_4$ hardly deliquesced but remained with its most common state being monohydrate particles.

Fig. 3 shows the Raman spectra of oxalic acid particles exposed to vapor as a function of relative humidity at 20 °C. Before humidifying, the Raman spectrum of oxalic acid dihydrate was recorded, as shown in Fig. 3 (gray dashed line). After being purged with dry N_2 for 2 h, these particles were exposed to vapor at varying relative humidity. As seen in Fig. 3A, peaks at 120, 158, 180, 486, 541, 847, 1320, 1486, and 1707 cm^{-1} were observed for dry particles, which was identical to the spectrum of anhydrous particles prepared by heating at 120 °C, indicating the formation of anhydrous oxalic acid. As RH increased above 31.4% RH, peak position shifts occurred. When RH reached 72.3%, peaks at 111, 158, 180, 486, 577, 642, 862, 1383, 1494, 1636, 1692, and 1738 cm^{-1} were observed. These peaks are identical to those of oxalic acid dihydrate, especially the appearance of peak at 111 cm^{-1} as the characteristic feature of oxalic acid dihydrate (Ebisuzaki and Angel, 1981). The detailed assignments were referenced to a previous study (Ma and He, 2012) and also summarized in Table 1. Moreover, as seen in Fig. 3B, peaks at 2585, 2770, and 2910 cm^{-1} due to anhydrous particles disappeared while peaks at 3445 and 3485 cm^{-1} appeared as RH increased above 31.4% RH. These results implied that anhydrous oxalic acid was converted to dihydrate particles in the range of 15.7–31.4% RH. The transition point is consistent with the vapor

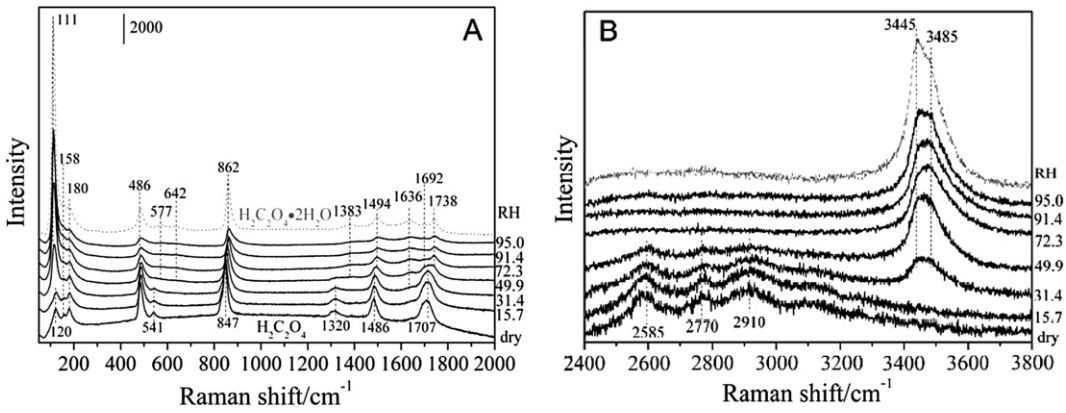

Fig. 3. Raman spectra of oxalic acid anhydrous particles exposed to vapor as a function of relative humidity at 20 °C. A) the range of 50–2000 cm^{-1}; B) the range of 2400–3800 cm^{-1}. The gray dashed line represents the Raman spectrum of oxalic acid dihydrate.

sorption analyzer results and also in good agreement with the results measured by Braban et al. (2003).

Raman spectra of $(NH_4)_2C_2O_4$ as a function of RH are shown in Fig. 4. As seen in Fig. 4A, several bands at 110, 174, 194, 450, 489, 652, 886, 1322, 1408, 1455, 1585, and 1728 cm^{-1} were observed for anhydrous particles. The detailed assignments are summarized in Table 1. No spectral change was observed below 50% RH. When RH increased from 50% to 60%, several band shifts were observed from 110 to 102, 174 to 165, 194 to 215, 489 to 495, and 886 to 900 cm^{-1}, respectively. The bands at 1408 and 1585 cm^{-1} disappeared while the band at 1728 cm^{-1} was split into two peaks at 1700 and 1746 cm^{-1}. A new band at 1614 was observed. These band features are identical to that of ammonium oxalate monohydrate (gray dashed line), indicating the conversion of anhydrous to monohydrate in the range of 50–60%. Fig. 4B shows the Raman spectra of N–H and O–H stretching modes of these particles during the humidifying process. The N–H stretching modes for anhydrous particles were observed at 3210, 3060, and 2896 cm^{-1}. When water was absorbed, the O–H stretching modes at 3030 and 3240 cm^{-1} were observed while the N–H stretching modes above 3000 cm^{-1} were overlapped (Frost, 2004). The transformation from anhydrous particles to the monohydrate of ammonium oxalate in the range of 50–60% RH is consistent with vapor sorption analyzer results. No deliquescence was observed for ammonium oxalate particles below 95% RH.

3.2.2. Calcium oxalate anhydrous and monohydrate

In the case of CaC_2O_4 particles, as shown in Fig. 5, the water content showed an abrupt increase at ~10% RH, at which point the molar ratio of calcium oxalate to water was close to unity. This implies that the transformation of anhydrous calcium oxalate to the monohydrate takes place at very low RH (~10%). After conversion to monohydrate, the water adsorption isotherm shows a curve similar to that of $CaC_2O_4 \cdot H_2O$ particles. For $CaC_2O_4 \cdot H_2O$ particles,

Table 1
Raman spectroscopic analysis of oxalic acid and oxalates.

$H_2C_2O_4$		$(NH_4)_2C_2O_4$		CaC_2O_4		FeC_2O_4		Mode	Ref.
Anhydrous	Dihydrate	Anhydrous	Monohydrate	Anhydrous	Monohydrate	Anhydrous	Dihydrate		
	3485, 3445		3240, 3030				3334	ν(O–H)	Frost (2004), Frost and Weier (2003)
		3210, 3060, 2896	2896					ν(N–H)	Frost (2004), Frost and Weier (2003)
2910, 2770, 2585								Combinations	Mohaček-Grošev et al. (2009)
1707	1738, 1692	1728	1746, 1700		1730	1684	1719	ν_a(C=O)	Frost (2004), Frost and Weier (2003)
	1636		1614		1632		1620	δ(HOH)	Ebisuzaki and Angel (1981); Mohaček-Grošev et al. (2009)
		1585						δ(HNH)?	
1486	1494	1475, 1455	1475, 1455	1491, 1464	1491, 1464	1492	1472	ν_a(C=O), ν_s(C–O) + ν(C–C)	Frost (2004), Frost and Weier (2003)
1320	1383	1408, 1322	1322		1400			ω(OCO)	Chang and Huang (1997)
847	862	886	900	896	941, 896, 868	930	923	ν_s(C–O) + δ (O–C=O) ν_s(C–O)/δ (O–C–O)	Frost (2004), Frost and Weier (2003)
541	642, 577	652	652	598	598		590	δ (O–C=O) + ν(M–O)	Frost (2004), Frost and Weier (2003)
486	486	489, 450	495, 450	503	503	531	531	ν(M–O)+ν(C–C) ring deform + δ(O–C=O) ν(M–O) + ring deform	Frost (2004), Frost and Weier (2003)
180	180	194	215	197	197	180	248	Out of plane bends	Frost (2004), Frost and Weier (2003)
158	158	174	165	165	141	117	209	Lattice modes	
120	111	110	102	108	108		117		

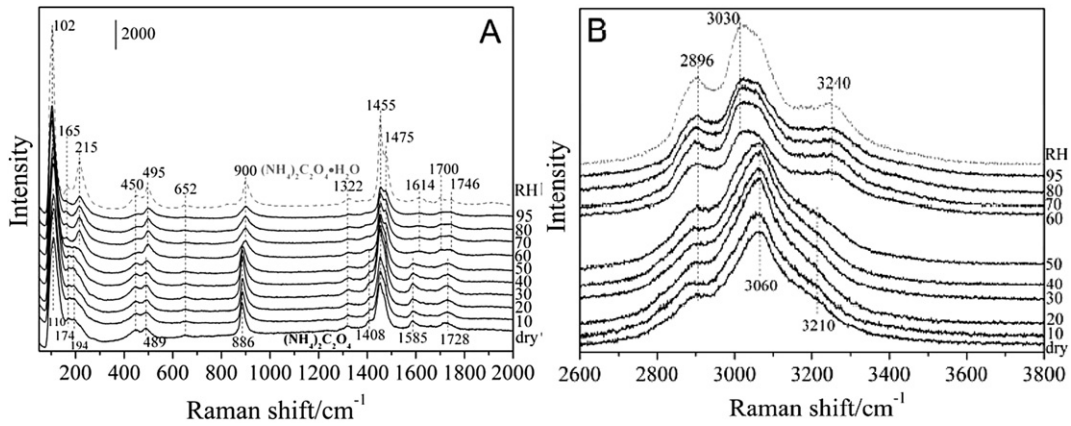

Fig. 4. Raman spectra of ammonium oxalate anhydrous particles exposed to vapor as a function of relative humidity at 20 °C. A) the range of 50–2000 cm^{-1}; B) the range of 2600–3800 cm^{-1}. The gray dashed line represents the Raman spectrum of ammonium oxalate monohydrate.

as shown in the inset in Fig. 5, the isotherm exhibits a multilayer adsorption type curve which can be fitted with the 3-parameter BET equation (Brunauer et al., 1938).

$$V = \left[\frac{V_m C \frac{P}{P_0}}{1-\frac{P}{P_0}}\right]\left[\frac{1-(n+1)\left(\frac{P}{P_0}\right)^n + n\left(\frac{P}{P_0}\right)^{n+1}}{1+(C+1)\frac{P}{P_0} - C\left(\frac{P}{P_0}\right)^{n+1}}\right] \quad (1)$$

where V is the volume of gas adsorbed at a relative pressure (P/P_0), and V_m is the volume of adsorbate constituting a monolayer of surface coverage. n is an adjustable parameter given as the maximum number of layers of the adsorbing gas. The BET C constant is related to the energy of adsorption in the first adsorbed layer. The relative humidity corresponding to monolayer adsorption for $CaC_2O_4 \cdot H_2O$ particles is determined to be ~18% RH. There are about 5–6 water layers at 90% RH and 11 water layers at 95% RH adsorbed on the surface of $CaC_2O_4 \cdot H_2O$ particles. Sullivan et al. (2009) reported that $CaC_2O_4 \cdot H_2O$ was significantly low CCN-active with apparent single-hygroscopicity parameter $\kappa = 0.05$, but not as inactive as its low solubility would predict. As shown here, although no deliquescence was observed, the water content for $CaC_2O_4 \cdot H_2O$ particles at high RH increased quickly which means that a liquid water film may form on the surface of particles. Therefore, $CaC_2O_4 \cdot H_2O$ may be activated under supersaturation conditions.

The Raman spectra of CaC_2O_4 exposed to water vapor are shown in Fig. 6. These anhydrous particles were prepared by heating samples at 220 °C and then cooling to room temperature under dry conditions. Several peaks at 1491, 1464, 896, 598, 503, 197, 165, and 108 cm^{-1} were observed for dry particles. As RH increased to 10% RH, several peaks at 1730, 1632, 1400, 941, 868, and 141 cm^{-1} were observed, which is similar to the spectrum of calcium oxalate monohydrate (gray dashed line), implying the formation of calcium oxalate monohydrate after the humidifying process (Chang and Huang, 1997). When RH was further increased, the peak at 165 cm^{-1} attributed to anhydrous particles disappeared, suggesting the complete conversion of CaC_2O_4 to $CaC_2O_4 \cdot H_2O$. Further change in the Raman spectra of hydrated CaC_2O_4 particles was not observed when RH was increased above 30%. This result is not unexpected since there was only surface adsorbed water on the surface of $CaC_2O_4 \cdot H_2O$ particles without deliquescence, as shown in the vapor sorption analyzer results (Fig. 5).

3.2.3. Iron oxalate anhydrous and dihydrate

Water adsorption isotherms of FeC_2O_4 and $FeC_2O_4 \cdot 2H_2O$ are shown in Fig. 7. They show that the water adsorption capacity of

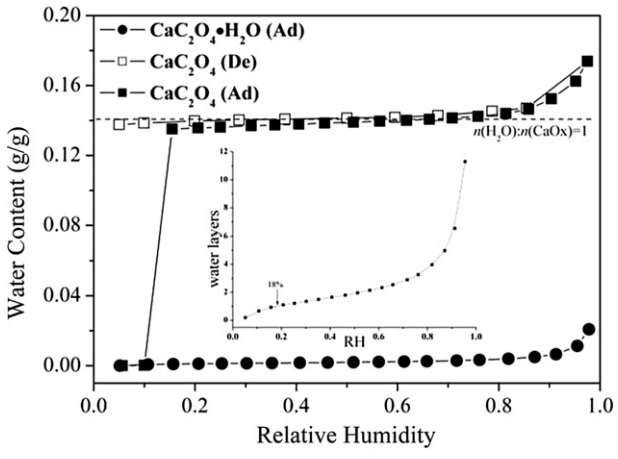

Fig. 5. Water adsorption–desorption isotherms of CaC_2O_4 and $CaC_2O_4 \cdot H_2O$ at 5 °C. Inset shows the fitted curve of the water isotherm of $CaC_2O_4 \cdot H_2O$.

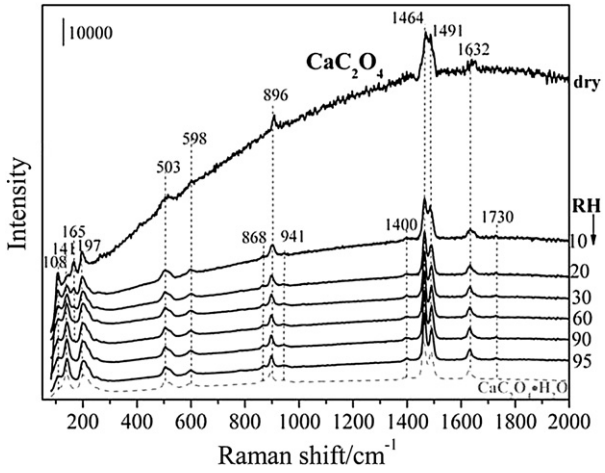

Fig. 6. Raman spectra of calcium oxalate anhydrous particles exposed to vapor as a function of relative humidity at 20 °C. The gray dashed line represents the Raman spectrum of calcium oxalate monohydrate.

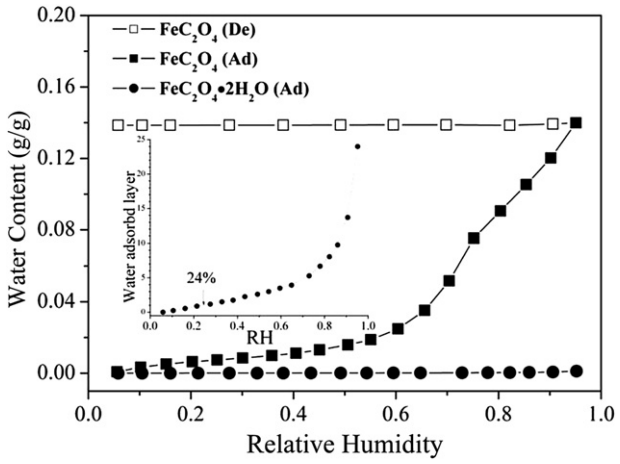

Fig. 7. Water adsorption–desorption isotherms of FeC_2O_4 and $FeC_2O_4{\cdot}2H_2O$ at 5 °C. Inset shows the fitted curve of the water isotherm of $FeC_2O_4{\cdot}2H_2O$.

$FeC_2O_4{\cdot}2H_2O$ is much smaller than FeC_2O_4. As seen in the inset in Fig. 7, the water adsorption isotherm of $FeC_2O_4{\cdot}2H_2O$ exhibits a multi-layer adsorption type curve. The relative humidity corresponding to monolayer adsorption for $FeC_2O_4{\cdot}2H_2O$ particles, calculated by Equation (1), is ~24% RH. There are about 7–8 layers water adsorbed on the surface of $FeC_2O_4{\cdot}2H_2O$ at 90% RH.

In the case of FeC_2O_4, the water adsorption isotherm also exhibits a multi-layer adsorption type curve at low humidity. It is interesting to note that a transition is exhibited at ~75% RH. When RH was above 75%, the slope of the isotherm decreased, indicating the depression of water adsorption capacity. Since the water adsorption capacity of $FeC_2O_4{\cdot}2H_2O$ is smaller than FeC_2O_4, the decrease of water adsorption amount above 75% RH may be due to the transformation of FeC_2O_4 to $FeC_2O_4{\cdot}2H_2O$. However, the water content at 75% RH is ~8%, which is less than 20%, the water content of $FeC_2O_4{\cdot}2H_2O$ particles. This suggests that the formation of dihydrate only occurs on the surface while the inner core of the particles is not involved.

Fig. 8 shows the Raman spectra of FeC_2O_4 exposed to vapor with various RH. For anhydrous FeC_2O_4 particles, several peaks at 117, 180, 209, 248, 531, 930, 1492, and 1684 cm^{-1} were observed. As RH increased, several peak position shifts occurred. When the RH was above 75% RH, peak position shifts were observed from 1492 to 1472, and 930 to 923 cm^{-1}, respectively. Meanwhile, two peaks at 180 and 1684 cm^{-1} disappeared and two peaks at 590 and 3334 cm^{-1} appeared. The appearance of the peak at 1472 cm^{-1} attributed to the symmetric stretching mode of OCO in oxalate and the peak at 3334 cm^{-1} attributed to the stretching mode of HOH indicated the production of $FeC_2O_4{\cdot}2H_2O$ particles during the humidifying process (Frost, 2004). However, the intensity of these peaks is lower than that in $FeC_2O_4{\cdot}2H_2O$ particles. Combined with the vapor sorption analyzer results, this confirmed that the conversion of anhydrous particles to hydrated particles was not complete but was limited to the surface.

3.3. Dehydration of oxalic acid and oxalates

Dehydration of oxalic acid and oxalates was conducted with the dehumidifying process. Desorption isotherms for $H_2C_2O_4$ and $(NH_4)_2C_2O_4$, CaC_2O_4, and FeC_2O_4 are shown in Figs. 2, 5, and 7, respectively. The water contents for hydrated $H_2C_2O_4$ and $(NH_4)_2C_2O_4$ particles showed an abrupt decrease at ~5% RH, indicating the dehydration of these particles. Meanwhile, no dehydration for hydrated CaC_2O_4 and FeC_2O_4 particles was observed. In addition, the Raman spectra of particles were recorded from 95% to 0% RH (data not shown). Both $CaC_2O_4{\cdot}H_2O$ and $FeC_2O_4{\cdot}2H_2O$ showed no change of spectra during the dehumidifying process even after dry N_2 flushing overnight, indicating no dehydration of these two particles under ambient conditions. For $H_2C_2O_4{\cdot}2H_2O$ and $(NH_4)_2C_2O_4{\cdot}H_2O$ particles, no change of spectra was observed when RH was higher than 5%RH. However, when they were purged with dry N_2, conversion of hydrate to anhydrous particles took place for both $H_2C_2O_4{\cdot}2H_2O$ and $(NH_4)_2C_2O_4{\cdot}H_2O$ particles. These results indicate that hydrated particles represent the most stable state for oxalic acid and oxalates in the atmosphere.

3.4. Assignments of Raman bands

Aqueous oxalate is uncoordinated and will be of point group D_{2d}. Thus the vibrational activity is given by $\Gamma = 3A1 + B1 + 2B1 + 3E$. All modes are Raman active and the $2B1 + 3E$ modes are infrared active. Upon coordination of the oxalate as a mono-oxalate species, the symmetry species is reduced to C_{2v} or D_{2h}. Assignments of Raman spectra of oxalic acid and oxalates have been reported in previous studies (Chang and Huang, 1997; D'Antonio et al., 2010; Ebisuzaki and Angel, 1981; Frost, 2004; Mancilla et al., 2009; Mohačeк-Grošev et al., 2009). According to these literatures, we made the assignments as follows, which are also summarized in Table 1. The bands in the range of 3000–3500 cm^{-1} are mainly assigned to the stretching mode of O–H in hydrated particles, which are 3485

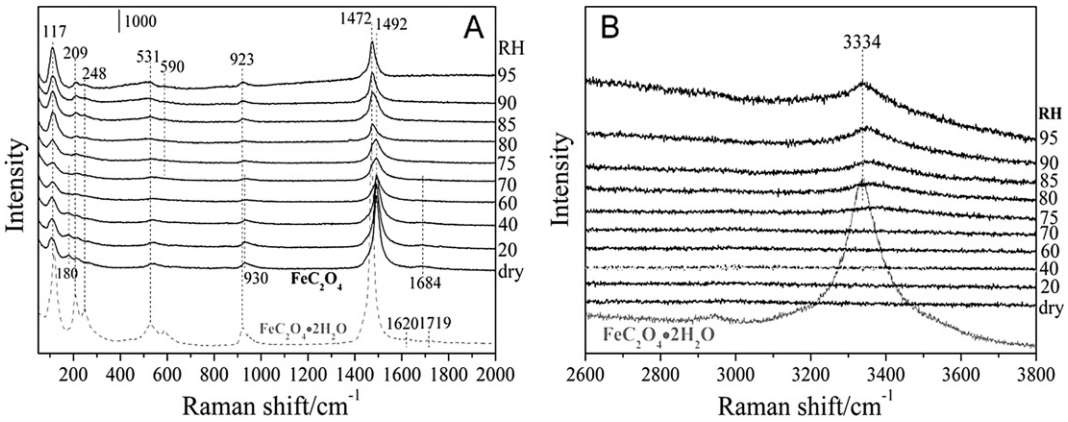

Fig. 8. Raman spectra of iron (II) oxalate anhydrous particles exposed to vapor as a function of relative humidity at 20 °C. A) the range of 50–2000 cm^{-1}; B) the range of 2600–3800 cm^{-1}. The gray dashed line represents the Raman spectrum of iron (II) oxalate dihydrate.

and 3445 cm^{-1} for $H_2C_2O_4 \cdot 2H_2O$, 3030 and 3240 cm^{-1} for $(NH_4)_2C_2O_4 \cdot H_2O$, and 3334 cm^{-1} for $FeC_2O_4 \cdot 2H_2O$, respectively. Three bands at 3210, 3060, and 2896 cm^{-1} for anhydrous $(NH_4)_2C_2O_4$ particles were attributed to the stretching modes of N–H (Frost, 2004). Three bands at 2585, 2770, and 2910 cm^{-1} were observed for $H_2C_2O_4$ anhydrous particles which may be due to band combinations (Mohaček-Grošev et al., 2009). The bands in the range of 1692–1750 cm^{-1} and 1450–1495 cm^{-1} were assigned to the stretching modes of C=O and C–O, respectively (Frost, 2004). Frost and Weier (2003) assigned the bands in the range of 1300–1390 cm^{-1} to the B3u OCO stretching mode. The bands around 900 cm^{-1} were assigned to the ν(C–C) stretching mode. The bands in the range of 200–700 cm^{-1} and below 200 cm^{-1} are due to combination and lattice modes, respectively (Ebisuzaki and Angel, 1981; Frost, 2004; Frost and Weier, 2003; Mancilla et al., 2009; Mohaček-Grošev et al., 2009).

Previous studies always assigned the Raman shift bands in the range of 1610–1650 cm^{-1} to the stretching mode of C=O (Frost, 2004; Mancilla et al., 2009). However, as shown here, these bands were only observed in hydrated particles but did not appear in anhydrous particles, e.g., 1636 cm^{-1} for $H_2C_2O_4 \cdot 2H_2O$, 1614 cm^{-1} for $(NH_4)_2C_2O_4 \cdot H_2O$, 1632 cm^{-1} for $CaC_2O_4 \cdot H_2O$, 1620 cm^{-1} for $FeC_2O_4 \cdot 2H_2O$. Combined with thermal analysis results, Chang and Huang (1997) assigned the band at 1635 cm^{-1} of CaC_2O_4 particles to the asymmetric stretching mode of C=O. However, it should be pointed out that the sample was measured in open air under natural convection in Chang and Huang (1997). In such a condition, anhydrous CaC_2O_4 particles are readily converted to $CaC_2O_4 \cdot H_2O$ according to its hygroscopicity. In a recent study, D'Antonio et al. (2010) showed that peaks at 1635 cm^{-1} were observed in the Raman spectrum of $MgC_2O_4 \cdot 2H_2O$ particles, while no band in the range of 1610–1650 cm^{-1} was observed for anhydrous MgC_2O_4 particles. It should also be noted that Ebisuzaki and Angel (1981) assigned the band at 1628 cm^{-1} in the spectrum of $(COOH)_2 \cdot 2H_2O$, which shifted to 1220 cm^{-1} for $(COOD)_2 \cdot 2D_2O$ particles. Thus, according to the hygroscopic behavior results in the present study, these bands in this range can be attributed to the bending mode of HOH.

4. Conclusions

In this study, the hygroscopic behavior of oxalic acid and oxalates, including $(NH_4)_2C_2O_4$, CaC_2O_4, and FeC_2O_4, was studied. Under ambient humidity conditions (5–95% RH), no deliquescence was observed for both oxalic acid and oxalates. The RH points for the conversion of anhydrous particles to hydrate were determined to be 20%, 55%, 10%, and 75% RH for $H_2C_2O_4$, $(NH_4)_2C_2O_4$, CaC_2O_4, and FeC_2O_4, respectively. Isotherms of hydrated Ca-oxalate and Fe-oxalate particles exhibit a multilayer adsorption type with capillary condensation at high RH (e.g. >90% RH). During the dehumidifying process, no dehydration for $CaC_2O_4 \cdot H_2O$ and $FeC_2O_4 \cdot 2H_2O$ to form CaC_2O_4 and FeC_2O_4 was observed, while $H_2C_2O_4 \cdot 2H_2O$ and $(NH_4)_2C_2O_4 \cdot H_2O$ were dehydrated to form $H_2C_2O_4$ and $(NH_4)_2C_2O_4$ below 5%RH. Humidifying and dehumidifying results indicate that hydrated particles represent the most stable state for oxalic acid and oxalates in the atmosphere.

Acknowledgment

This research was funded by the "Strategic Priority Research Program-Formation mechanism and control strategies of haze in China" of the Chinese Academy of Sciences (Grant No. XDB05010300) and National Natural Science Foundation of China (20937004 and 21107129)."

References

Braban, C.F., Carroll, M.F., Styler, S.A., Abbatt, J.P.D., 2003. Phase transitions of malonic and oxalic acid aerosols. Journal of Physical Chemistry A 107, 6594–6602.
Brunauer, S., Emmett, P.H., Teller, E., 1938. Adsorption of gases in multimolecular layers. Journal of the American Chemical Society 60, 309–319.
Carlton, A.G., Turpin, B.J., Altieri, K.E., Seitzinger, S., Reff, A., Lim, H.J., Ervens, B., 2007. Atmospheric oxalic acid and SOA production from glyoxal: results of aqueous photooxidation experiments. Atmospheric Environment 41, 7588–7602.
Chang, H., Huang, P.J., 1997. Thermal decomposition of $CaC_2O_4 \cdot H_2O$ studied by Thermo-Raman spectroscopy with TGA/DTA. Analytical Chemistry 69, 1485–1491.
Charlson, R.J., Schwartz, S.E., Hales, J.M., Cess, R.D., Coakley, J.A., Hansen, J.E., Hofmann, D.J., 1992. Climate forcing by anthropogenic aerosols. Science 255, 423–430.
Chebbi, A., Carlier, P., 1996. Carboxylic acids in the troposphere, occurrence, sources, and sinks: a review. Atmospheric Environment 30, 4233–4249.
D'Antonio, M.C., Mancilla, N., Wladimirsky, A., Palacios, D., González-Baró, A.C., Baran, E.J., 2010. Vibrational spectra of magnesium oxalates. Vibrational Spectroscopy 53, 218–221.
Dong, J.L., Xiao, H.S., Zhao, L.J., Zhang, Y.H., 2009. Spatially resolved Raman investigation on phase separations of mixed $Na_2SO_4/MgSO_4$ droplets. Journal of Raman Spectroscopy 40, 338–343.
Ebisuzaki, Y., Angel, S.M., 1981. Raman study of hydrogen bonding in α and β-oxalic acid dihydrate. Journal of Raman Spectroscopy 11, 306–311.
Edwards, H.G.M., Seaward, M.R.D., Attwood, S.J., Little, S.J., de Oliveira, L.F.C., Tretiach, M., 2003. FT-Raman spectroscopy of lichens on dolomitic rocks: an assessment of metal oxalate formation. Analyst 128, 1218–1221.
Ervens, B., Feingold, G., Frost, G.J., Kreidenweis, S.M., 2004. A modeling study of aqueous production of dicarboxylic acids: 1. Chemical pathways and speciated organic mass production. Journal of Geophysical Research 109, D15205.
Frost, R.L., 2004. Raman spectroscopy of natural oxalates. Analytica Chimica Acta 517, 207–214.
Frost, R.L., Weier, M.L., 2003. Raman spectroscopy of natural oxalates at 298 and 77 K. Journal of Raman Spectroscopy 34, 776–785.
Furukawa, T., Takahashi, Y., 2011. Oxalate metal complexes in aerosol particles implications for the hygroscopicity of oxalate-containing particles. Atmospheric Chemistry and Physics 11, 4289–4301.
Garty, J., Garty-Spitz, R.L., 2011. Neutralization and neoformation: analogous processes in the atmosphere and in lichen thalli-a review. Environmental and Experimental Botany 70, 67–79.
Hsieh, L.Y., Kuo, S.C., Chen, C.L., Tsai, Y.I., 2007. Origin of low-molecular-weight dicarboxylic acids and their concentration and size distribution variation in suburban aerosol. Atmospheric Environment 41, 6648–6661.
IPCC, 2007. Climate Change 2007: the Physical Science Basis. In: Contribution of Working Group I to the Fourth Assessment Report of the Intergovernmental Panel on Climate Change.
Kawamura, K., Imai, Y., Barrie, L.A., 2005. Photochemical production and loss of organic acids in high Arctic aerosols during long-range transport and polar sunrise ozone depletion events. Atmospheric Environment 39, 599–614.
Kerminen, V.-M., Ojanen, C., Pakkanen, T., Hillamo, R., Aurela, M., Meriläinen, J., 2000. Low-molecular-weight dicarboxylic acids in an urban and rural atmosphere. Journal of Aerosol Science 31, 349–362.
Kawamura, K., Barrie, L.A., Desiree, T.-S., 2010. Intercomparison of the measurements of oxalic acid in aerosols by gas chromatography and ion chromatography. Atmospheric Environment 44, 5316–5319.
Kumar, P.P., Broekhuizen, K., Abbatt, J.P.D., 2003. Organic acids as cloud condensation nuclei: laboratory studies of highly soluble and insoluble species. Atmospheric Chemistry and Physics 3, 509–520.
Kundu, S., Kawamura, K., Andreae, T.W., Hoffer, A., Andreae, M.O., 2010. Molecular distributions of dicarboxylic acids, ketocarboxylic acids and a-dicarbonyls in biomass burning aerosols: implications for photochemical production and degradation in smoke layers. Atmospheric Chemistry and Physics 10, 2209–2225.
Liu, Y.C., Liu, C., Ma, J.Z., Ma, Q.X., He, H., 2010. Structural and hygroscopic changes of soot during heterogeneous reaction with O_3. Physical Chemistry Chemical Physics 12, 10896–10903.
Ma, Q.X., He, H., 2012. Synergistic effect in the humidifying process of atmospheric relevant calcium nitrate, calcite and oxalic acid mixtures. Atmospheric Environment 50, 97–102.
Ma, Q.X., Liu, Y.C., He, H., 2010. The utilization of physisorption analyzer for studying the hygroscopic properties of atmospheric relevant particles. Journal of Physical Chemistry A 114, 4232–4237.
Mancilla, N., D'Antonio, M.C., González-Baró, A.C., Baran, E.J., 2009. Vibrational spectra of lead (II) oxalate. Journal of Raman Spectroscopy 40, 2050–2052.
Mochida, M., Kawabata, A., Kawamura, K., Hatsushika, H., Yamazaki, K., 2003a. Seasonal variation and origins of dicarboxylic acids in the marine atmosphere over the western North Pacific. Journal of Geophysical Research 108, 4193.
Mochida, M., Umemoto, N., Kawamura, K., Uematsu, M., 2003b. Bimodal size distribution of C2-C4 dicarboxylic acids in the marine aerosols. Geophysical Research Letters 30, 1672.

Mohaček-Grošev, V., Grdadolnik, J., Stare, J., Hadži, D., 2009. Identification of hydrogen bond modes in polarized Raman spectra of single crystals of α-oxalic acid dihydrate. Journal of Raman Spectroscopy 40, 1605–1614.
Peng, C.G., Chan, C.K., 2001. The water cycles of water-soluble organic salts of atmospheric importance. Atmospheric Environment 35, 1183–1192.
Peng, C.G., Chan, M.N., Chan, C.K., 2001. The hygroscopic properties of dicarboxylic and multifunctional acids: measurements and UNIFAC predictions. Environmental Science & Technology 35, 4495–4501.
Prenni, A.J., DeMott, P.J., Kreidenweis, S., Sherman, D.E., Russell, L.M., Ming, Y., 2001. The effects of low molecular weight dicarboxylic acids on cloud formation. Journal of Physical Chemistry A 105, 11240–11248.
Ramanathan, V., Crutzen, P.J., Kiehl, J.T., Rosenfeld, D., 2001. Aerosols, climate, and the hydrological cycle. Science 294, 2119–2124.
Röhrl, A., Lammel, G., 2001. Low-molecular weight dicarboxylic acids and glyoxylic acid: seasonal and air mass characteristics. Environmental Science & Technology 35, 95–101.
Sorooshian, A., Lu, M.L., Brechtel, F.J., Jonsson, H., Feingold, G., Flagan, R.C., Seinfeld, J.H., 2007. On the source of organic acid aerosol layers above clouds. Environmental Science & Technology 41, 4647–4654.
Sorooshian, A., Varutbangkul, V., Brechtel, F.J., Ervens, B., Feingold, G., Bahreini, R., Murphy, S.M., Holloway, J.S., Atlas, E.L., Buzorius, G., Jonsson, H., Flagan, R.C., Seinfeld, J.H., 2006. Oxalic acid in clear and cloudy atmospheres: analysis of data from International Consortium for Atmospheric Research on Transport and Transformation 2004. Journal of Geophysical Research 111, D23S45.
Sullivan, R.C., Moore, M.J.K., Petters, M.D., Kreidenweis, S.M., Roberts, G.C., Prather, K.A., 2009. Effect of chemical mixing state on the hygroscopicity and cloud nucleation properties of calcium mineral dust particles. Atmospheric Chemistry and Physics 9, 3303–3316.
Sullivan, R.C., Prather, K.A., 2007. Investigations of the diurnal cycle and mixing state of oxalic acid in individual particles in Asian aerosol outflow. Environmental Science & Technology 41, 8062–8069.
Wang, G., Xie, M., Hu, S., Gao, S., Tachibana, E., Kawamura, K., 2010. Dicarboxylic acids, metals and isotopic compositions of C and N in atmospheric aerosols from inland China: implications for dust and coal burning emission and secondary aerosol formation. Atmospheric Chemistry and Physics 10, 6087–6096.
Warneck, P., 2003. In-cloud chemistry opens pathway to the formation of oxalic acid in the marine atmosphere. Atmospheric Environment 37, 2423–2427.
Wu, Z.J., Nowak, A., Poulain, L., Herrmann, H., Wiedensohler, A., 2011. Hygroscopic behavior of atmospherically relevant water-soluble carboxylic salts and their influence on the water uptake of ammonium sulfate. Atmospheric Chemistry and Physics 11, 12617–12626.
Yang, F., Chen, H., Wang, X.N., Yang, X., Du, J.F., Chen, J.M., 2009. Single particle mass spectrometry of oxalic acid in ambient aerosols in Shanghai: mixing state and formation mechanism. Atmospheric Environment 43, 3876–3882.
Yang, L.M., Yu, L.E., 2008. Measurements of oxalic acid, oxalates, malonic acid, and malonates in atmospheric particulates. Environmental Science & Technology 42, 9268–9275.
Yao, X.H., Fang, M., Chan, C., Ho, K.F., Lee, S.C., 2004. Characterization of dicarboxylic acids in PM2.5 in Hong Kong. Atmospheric Environment 38, 963–970.
Yao, X.H., Fang, M., Chan, C.K., 2002. Size distributions and formation of dicarboxylic acids in atmospheric particles. Atmospheric Environment 36, 2099–2107.
Yu, J.Z., Huang, X.F., Xu, J.H., Hu, M., 2005. When aerosol sulfate goes up, so does oxalate: implication for the formation mechanisms of oxalate. Environmental Science & Technology 39, 128–133.
Yu, S.C., 2000. Role of organic acids (formic, acetic, pyruvic and oxalic) in the formation of cloud condensation nuclei (CCN): a review. Atmospheric Research 53, 185–217.